International Symposium COMODIA 90: 405-410(1990)

The Effect of Swirl on the Decay and Generation of In-Cylinder Turbulence during the Compression Stroke

Y.Moriyoshi, H.Ohtani, M.Yagita and T.Kamimoto

Tokyo Institute of Technology
12-1, Ohokayama 2-chome
Megro-ku, Tokyo 152
Japan

ABSTRACT

The lateral turbulence integral length scales of the axial and tangential velocity components were measured using a two-point, single-probe-volume, laser Doppler velocimetry system in a motored single-cylinder internal combustion engine. The measurements were carried out on an axisymmetric transparent cylinder engine with a pancake-shaped chamber during the period spanning the intake and expansion strokes at an engine speed of 320rpm for three different swirl ratios. The results obtained for this engine indicate that in the case of no swirl, the turbulence intensity and the integral length scale decrease monotonously from compression stroke to expansion stroke, while in the presence of swirl, they happen to increase during the compression stroke as affected by the vortex ring generated by an interference between the swirl and piston motion.

1. INTRODUCTION

Since turbulence intensity and the length scale of in-cylinder flow of engines have strong effects on combustion in reciprocating engines, there have been many experimental and theoretical studies on turbulence in the cylinder.

Previous experiments show that the turbulence intensity tends to decrease with time during the compression and expansion strokes with a pancake-shaped combustion chamber (1-3). The integral length scale of turbulence has been measured by means of multi-point simultaneous LDV measurements (3-7). However, the results reported so far are not necessarily consistent.

In this study, the turbulence intensity and lateral integral length scale of turbulence of an in-cylinder flow of a transparent model engine are measured by means of the spatial correlation method of Fraser and Bracco (6,7) using an LDV system at motoring operation during intake, compression and expansion strokes. The effect of swirl ratio on spacial and temporal variations of turbulence intensity, length scale and degrees of the homogeneity or isotropy of turbulence are examined.

2. EXPERIMENTAL METHOD

2.1 Experimental Apparatus

The model engine has a centered single valve and allows an axi-symmetrical flow field (2). The cylinder liner made of quartz facilitates LDV application to the whole space inside the cylinder. The specifications are; bore x stroke = ϕ80mm x 80mm, the top clearance height 20mm, the compression ratio 5.0, valve diameter 32mm and the maximum valve-lift 8.4mm. The engine was motored at 320rpm. The swirl ratio defined as the value at the intake valve-closing-time (210 degrees ATDC) was changed as 0, 1.5 and 3.6 using a swirler incorporated in the intake passage.

Figure 1 shows the single probe-volume with two-point LDV system (6,7). In this technique, the measurement of velocities at two points separated at a certain distance requires elongation of the length of the probe-volume. Then, a condenser lens with 592mm focal distance and a beam separation of 22mm were employed, resulting in a crossing half-angle of 1.06° and a length of the probe-volume of 10.5mm ($1/e^2$). The real image of the probe-volume was projected outside of the cylinder with a magnifying power of one and scattered light from the two points were detected by two quartz optical fibers (core diameter 0.40mm) respectively. One fiber was fixed and the other was moved by a precise traverse mechanism which makes use of a micrometer. The separation of two fibers were set at 0.0, 0.50, 1.00, 2.00 - 9.00mm (1.00mm interval). The two incident beams cross on a line which meets at the right angle to the cylinder axis.

The measurements were made at 4 points. r and z refer to the radial distance from the cylinder-axis and axial distance from the cylinder head respectively. The locations of the fixed points are (r,z)=(5,10), (15,10), (25,10) and (5,16) [unit:mm].

For signal processing a tracker (KANOMAX Model 8015) and a flow analyzer (TSI IFA-550) were employed, and silicone oil particles (diameter of 4μm) were used as the scattering particles.

The output signals from the signal processors and logical output from a coincidence detector to judge the simultaneity of two signals were both A/D-converted at every 0.36 crank-angle degree and transferred to a computer (HP 9836A) and then stored in a hard disk unit. The calculations of cross-correlation were executed on a workstation (HP 318M). It took about 30 minutes for one measurement point.

2.2 Definition of Turbulence

The mean velocity for each cycle was defined as the moving-averaged velocity for each cycle, and the

difference between the instantaneous velocity and the mean velocity was determined as the turbulence component. The cut-off frequency (f_c) to be used in the calculation of the moving-averaged velocity was investigated by the power spectrum analysis of the ensemble-averaged mean velocity during a period from the latter half of the intake stroke to the early half of the expansion stroke. The frequency (f_{90}) under which the integrated power includes 90% of total power was decided as the standard cut-off frequency (2). Two different cut-off frequencies f_c of 50Hz (-3dB, corresponding to 17.64 degrees in crank-angle) and 25Hz (34.2 degrees) were selected.

2.3 Data Processing Method

2.3.1 Simultaneity of velocity measurement at two points. For calculating the spacial correlation it is necessary for two signals to be detected simultaneously and then, it was examined how much time difference is allowable for two signals. The time period or window width during which two different signals arrive was changed as 5, 20, 30 and 50μs and then, in each case both the spacial correlation coefficient and the data rate, which accounts for the valid signals included in the window, are investigated. Fig. 2 represents the results when the axial velocities were measured at two points with a separation of 4mm. The correlation coefficient and its standard deviation, σ, at a crank angle interval from 165 to 175 degrees ATDC(Intake TDC) are calculated with 700 sampled data using a cut-off frequency f_c of 25Hz. As shown in the figure the window width of 20μs appears the best choice because the correlation coefficient is very close to that for the window width of 5μs and because the data rate is sufficiently high. The similar trend was observed for the case when a cut-off frequency of 50Hz was employed and as a result, we decided to adopt the window width of 20μs in our experiments. About 1000 samples taken over 160 cycles were used for calculating a correlation coefficient.

2.3.2 Method to calculate the lateral integral length scale of turbulence. The spacial correlation coefficient of turbulence, R(r), was calculated from 84.78 to 457.74 degrees ATDC at 37 sections having a period of 10.08 degrees.

Suppose the two locations at r_1 and r_2 respectively, the spacial correlation coefficient of turbulence can read as in Eq.(1);

$$R(r_1, r_2) = \frac{1}{N} \sum_{i=1}^{N} \frac{u_i'(r_1) \cdot u_i'(r_2)}{u'\mathrm{rms}(r_1) \cdot u'\mathrm{rms}(r_2)} \quad \cdots (1)$$

where, i refers to i-th measured value, N the number of samples, u' turbulence velocity and u'rms turbulence intensity.

The correlation coefficient should be unity when the distance between the two locations is zero. Owing to the difference in characteristics between the two signal processors employed, however, the value is not necessarily unity. Then, a correction method was proposed to remove such an error: Output from an optical fiber was processed with two signal processors and two turbulence velocities of $u_z'(r_1)$, $u_z'(r_2)$ were obtained. (In this case, $r_1=r_2$). Plotting $u_z'(r_1)$ and $u_z'(r_2)$ of axial velocities at $(r,z)=(15,10)$ onto the ordinate and the abscissa respectively makes a scatter plot shown in Fig. 3. An ellipse, indicating by a broken line, has a major axis and a minor axis with each tripled value of standard deviation of $(u_z'(r_1) + u_z'(r_2))$ and $(u_z'(r_1) - u_z'(r_2))$ respectively. Data plotted outside of the ellipse which accounts for 2% of the total data were removed as noise from data. The correlation coefficient was calculated to be 0.81 in this example. Now, let us denote that the difference between two turbulence velocities processed with two different processors at the same point as u_{di}, the number of samples as N. A correction factor of $u_d^2=(\Sigma u_{di}^2)/N$ can be calculated on the assumption that $u_{di}=0$ for large N. Substituting u_d^2 into Eq.(2), we can get the corrected correlation coefficient whose value is close to unity.

$$R'(r_1, r_2) = \frac{1}{N} \sum_{i=1}^{N} \frac{u_i'(r_1) \cdot u_i'(r_2)}{\sqrt{(u'\mathrm{rms}(r_1)^2 - u_d^2)} \cdot u'\mathrm{rms}(r_2)} \quad \cdots (2)$$

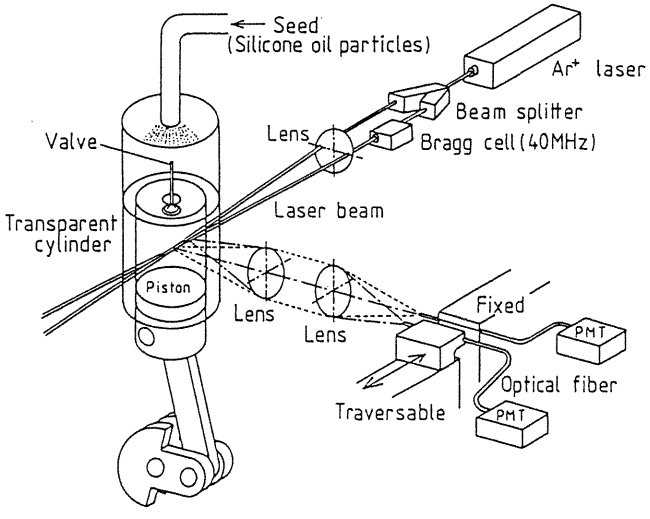

Fig. 1 LDV sytem for turbulent length scale measurement

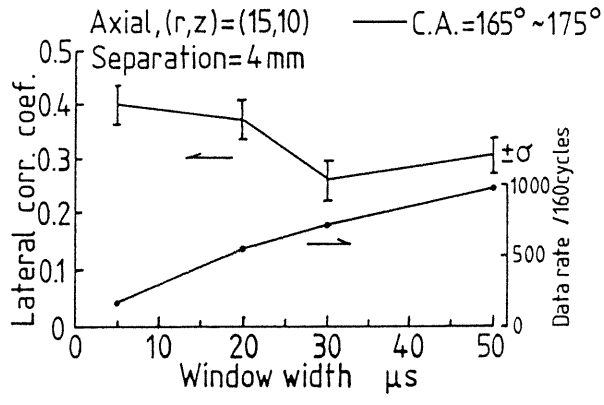

Fig. 2 Variations with window width of correlation coefficient and data rate (S.R.=3.6, fc=25Hz)

Correlation coefficients at two separated locations were corrected at each section using the value of u_d^2 obtained for zero separation. So as to elucidate the validity of this method, variations with time of u_d^2 at three points of (r,z)=(5,10), (15,10) and (25,10) with a swirl ratio 1.5 are shown in Fig. 4. It shows that the difference in u_d^2 among the three positions is large during the intake stroke, but the difference becomes small during the compression and expansion strokes. This means that the proposed correction method is appropriate during the compression and expansion strokes. In addition, R'(r) is curve-fitted using Eq.(3) by the least squares method;

$$R'(r) = \exp(-A \cdot r) \cdot \cos(B \cdot r) \quad \text{---- (3)}$$

where, A and B are constants and in this figure, r designates the separation. Fig. 5 shows an example of three correlation coefficients of original, corrected and curve-fitted at (r,z)=(5,10) during 296.46 ~ 306.54 degrees ATDC. Integration of R'(r) from 0 to r^* where the curve-fitted curve first crosses zero yields the integral lateral length scale of turbulence, L_g. In this example, L_g is 2.02mm.

$$L_g = \int_0^{r^*} R'(r)\, dr \quad \text{----------} \quad (4)$$

The length scale in the axial direction and that in the tangential direction are designated as L_{gz} and $L_{g\theta}$ respectively.

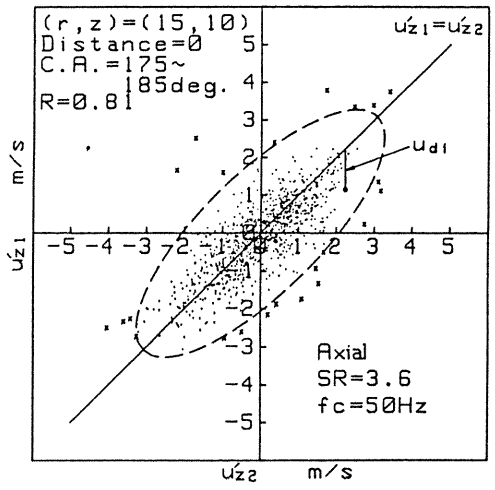

Fig. 3 Scatter plots of turbulence velocity

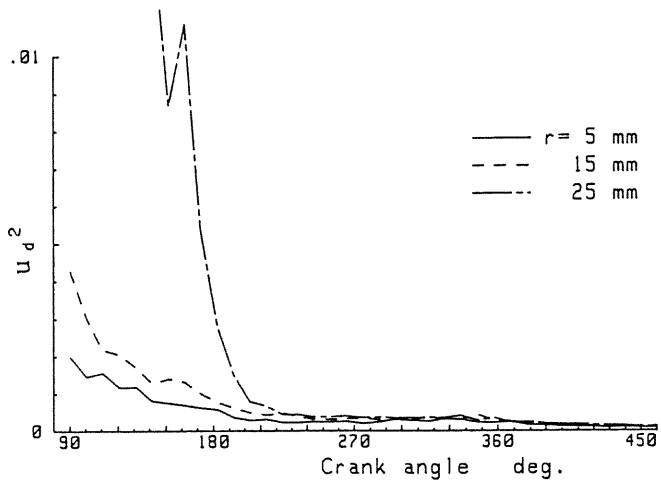

Fig. 4 Variations with time of correction factor

3. RESULTS AND DISCUSSION

3.1 Effects of Swirl Ratio

First of all the flow fields subject to experiments are presented in Figs. 6 and 7. Fig. 6 shows radial profiles of the ensemble-averaged tangential mean velocity, U_θ, at the compression TDC for three different swirl ratios. Fig. 7 also shows radial profiles of turbulence intensities of both tangential component, u'_θrms, and axial component, u'_zrms.

Fig. 8 shows variations with time of turbulence intensity at three radial locations of r=5, 15, 25mm in z=10mm plane with the swirl ratio as a parameter. Fig. 9 shows variations with time of L_{gz} and $L_{g\theta}$ at the same locations as in Fig. 8. Fig. 10 shows variations with time of L_{gz} and $L_{g\theta}$ at (r,z)=(5,16) for both cut-off frequencies of f_c=25Hz and 50Hz.

3.1.1 In the case of swirl ratio 0. As shown in Fig. 8(a), turbulence intensities of both axial and tangential direction from the compression to the expansion stroke decrease monotonously at each location. This implies that the dissipation of turbulence is dominant during this period. From the intake-valve-closing time through the early half of the expansion stroke, the turbulence intensity takes almost the same value for the axial and the tangential components.

According to Figs. 9(a) and 10(a), both L_{gz} and $L_{g\theta}$ decrease monotonously from the compression to the expansion stroke (4) at each location. Besides, L_{gz} and $L_{g\theta}$ have almost equal magnitude, and during

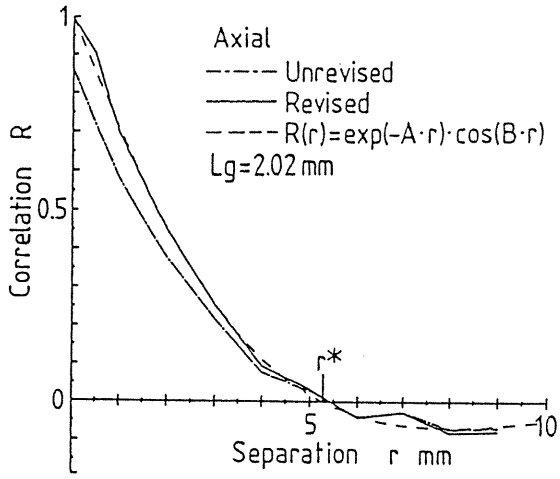

Fig. 5 Correlation coefficient versus separation at (r,z)=(5,10) (C.A.=300°, S.R.=3.6, fc=25Hz)

the same period, L_{gz} and $L_{g\theta}$ are almost equal regardless of radial location. As the radial profile of turbulence intensity shown in Fig. 7 is almost homogeneous, turbulence around the compression TDC seems to be isotropic and homogeneous in the case of swirl ratio 0.

The length scales calculated with different cut-off frequencies are compared as shown in Fig. 10(a), but no qualitative difference is observed between two cases.

3.1.2 In the case of swirl ratio 1.5. In this case, the tangential mean velocity takes a profile like a solid vortex as shown in Fig. 6. Fig. 8(b) shows that except for the large turbulence intensity of the axial component during the intake stroke at location (r,z)=(25,10), turbulence intensities of the axial and the tangential components exhibit almost equal values at each radial location during a period from the intake-valve-closing time to the first half of the expansion stroke.

It is worth to note that the axial turbulence intensity hardly decreases during the compression stroke and it takes a faint maximum value in the latter half of the expansion stroke (7). At the same time both L_{gz} and $L_{g\theta}$ show maximum values respectively in the latter half of the compression stroke as Figs. 9(b) and 10(b) show. In order to investigate this reason, axi-symmetrical numerical calculations using a modified k-ε turbulence model were made with measured velocities at 270 or 260 degrees ATDC (8,9) as initial conditions. Calculated velocity vector maps at 300 degrees ATDC at the r-z cross section are shown in Fig. 11. The mathematical model used has been validated in a comparison between calculated and experimental results in our previous work (9). It is obvious from Fig. 11(a) that a large-scale secondary flow, which was not generated in the case of swirl ratio 0, developes during the compression stroke at the r-z cross section. This flow transports and generates turbulence and then, it can be supposed that turbulence intensity and length scale take respective maximum values in the compression stroke. After showing maximum values during the compression stroke both L_{gz} and $L_{g\theta}$ decrease toward TDC due to the effect of compression.

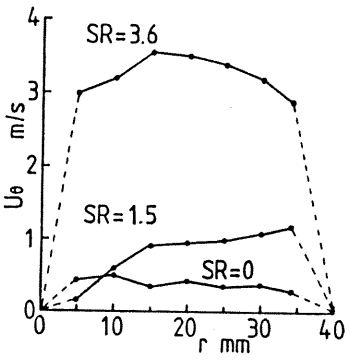

Fig. 6 Radial profile of ensemble-averaged tangential mean velocity (z=10mm)

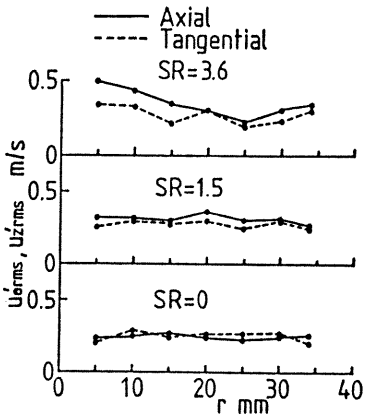

Fig. 7 Radial profile of turbulence intensities of both tangential and axial components at TDC

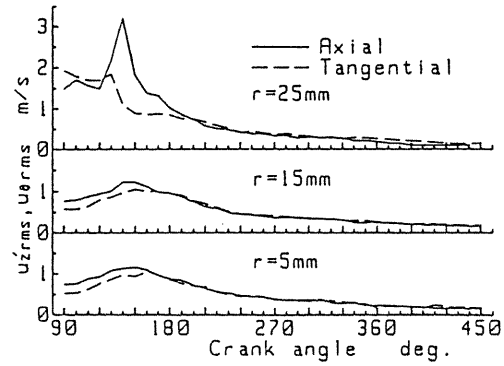

(a) S.R.=0 (fc=50Hz)

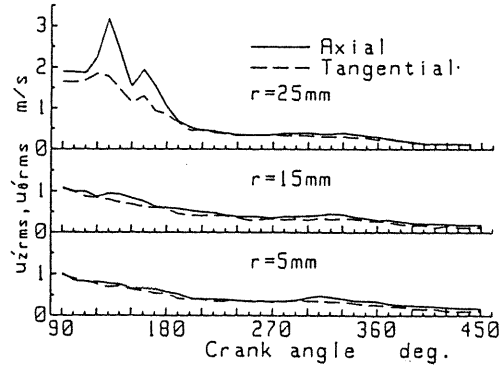

(b) S.R.=1.5 (fc=50Hz)

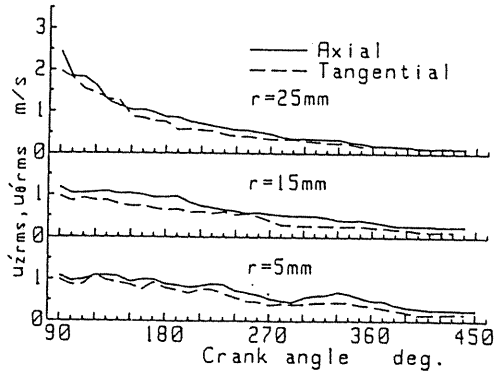

(c) S.R.=3.6 (fc=50Hz)

Fig. 8 Turbulence intensity versus crank angle (z=10mm)

Figures 9(b) and 10(b) also show that around the compression TDC, L_{gz} and $L_{g\theta}$ are almost equal for the case of f_c=25Hz. From the equality of axial and tangential component of both intensity and scale of turbulence, we can conclude that the turbulence field defined as a component having frequencies higher than 50Hz is isotropic. However, vortices having a low frequency component from 25 to 50Hz is obviously anisotropic because as Fig. 10(b) shows, L_{gz} and $L_{g\theta}$ measured with a cut-off frequency of 25Hz do not coincide each other.

3.1.3 In the case of swirl ratio 3.6. In this case, as shown in Fig. 6 the tangential mean velocity profile is like a Rankine vortex which consists of a solid and a free vortices. Let us see first the turbulence behavior in a cross section of z=10mm. As for turbulence scales, Fig. 9(c) indicates that both L_{gz} and $L_{g\theta}$ show almost equal

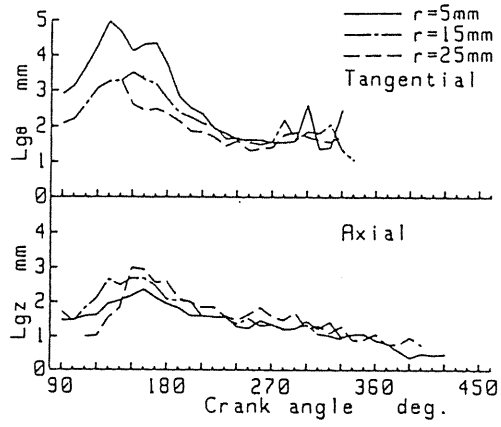

(a) S . R . = 0

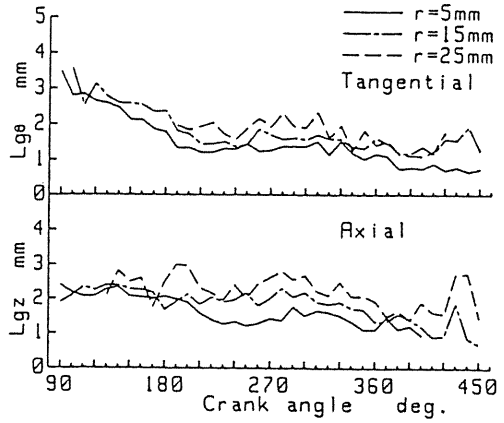

(b) S . R . = 1 . 5

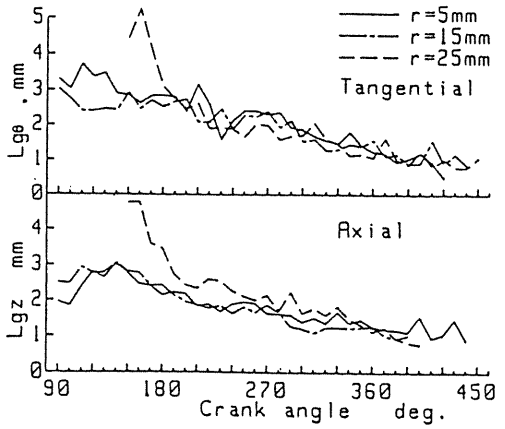

(c) S . R . = 3 . 6

Fig. 9 L_{gz}, $L_{g\theta}$ versus crank angle (z=10mm, fc=50Hz)

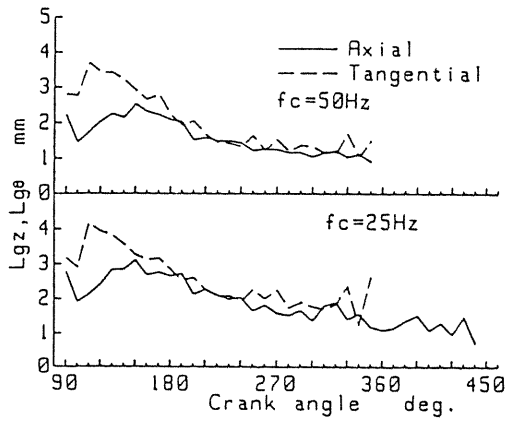

(a) S . R . = 0

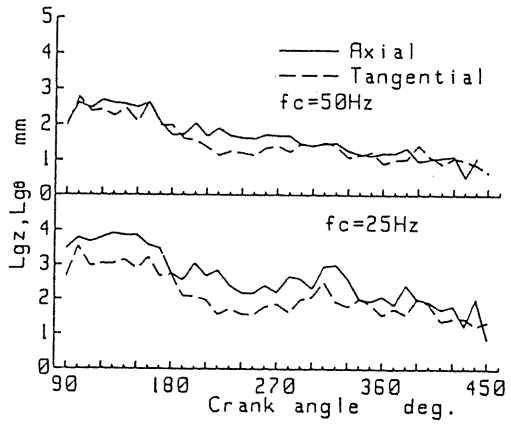

(b) S . R . = 1 . 5

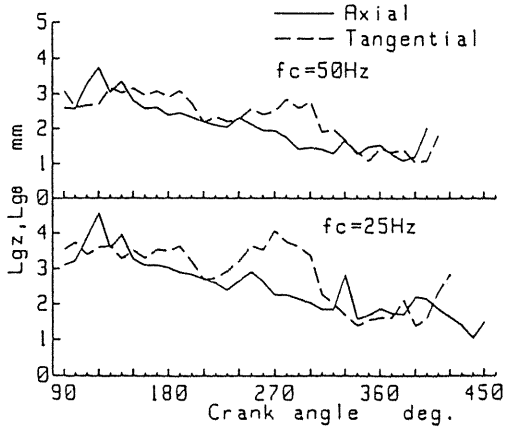

(c) S . R . = 3 . 6

Fig. 10 L_{gz}, $L_{g\theta}$ versus crank angle at (r,z)=(5,16) (fc=25Hz, fc=50Hz)

changes and decrease monotonously from the compression to the first half of the expansion stroke. However as Fig. 8(c) shows the turbulence intensity of the axial component is larger than that of the tangential component in the whole period. And then, turbulence can be regarded as anisotropic. The turbulence intensity decreases monotonously with time as a whole, but at a location of r=5mm the axial turbulence intensity takes a maximum value during the latter half of the compression stroke as in the case of swirl ratio of 1.5.

Next the turbulence field in a cross section of z=16mm away further from the cylinder head surface was investigated. Fig. 10(c) shows the variations with time of integral length scales at (r,z)=(5,16) mm. One can notice again that $L_{g\theta}$ has a maximum value around 270 degrees ATDC in the compression stroke. To investigate this, the calculated flow field in the r-z cross section is also illustrated in Fig. 11(b). A large-scale secondary flow observed in the case of swirl ratio 1.5 is not developed in this case, but a ring vortex is observed in a region around the cylinder center. Thus the calculation elucidates clearly the experimental results that generation and transportation of turbulence are limited in a region around the center and dissipation dominates outside of the vortex.

4. CONCLUSIONS

The lateral length scale and intensity of turbulence of an axi-symmetrical in-cylinder flow of a transparent model engine were measured by means of the single volume two-point LDV system at 320rpm motoring operation. Regarding the generation and dissipation of turbulence during the compression and the expansion strokes, following conclusions were acquired:

(1) In the absence of swirl, the turbulence intensity decreases and the turbulence length scale also decreases with time. It is possible to explain that this is because the dissipation of turbulence dominates the variation with time of the turbulence characteristic. A minimum value of the turbulence length scale at the compression TDC, which was reported in previous studies (1,3), was not observed.

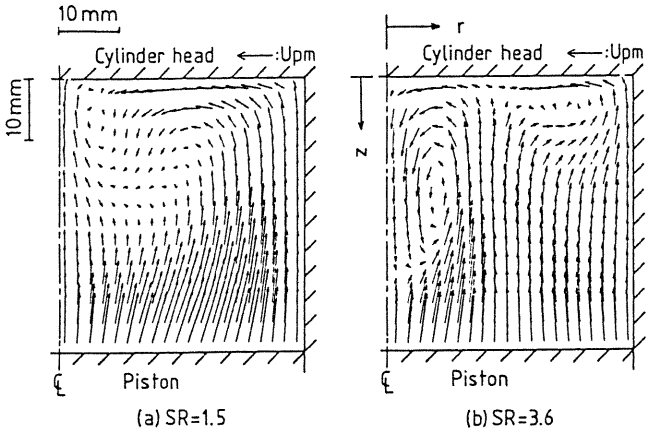

Fig. 11 Mean velocity vector in r-z section by numerical calculation
(300° ATDC, Upm: Mean piston speed)

(2) In the case of swirl ratio of 1.5 which has a solid vortex type swirl profile, both the intensity and length scales of turbulence increase and take maximum values in the compression stroke at some measuring points. A multidimensional calculation conducted using the measured initial conditions attributed this phenomena to the facts that a large-scale secondary flow is developed in the cylinder by an interference between the swirl and piston motion during the compression stroke and that this flow generates and transports turbulence.

(3) In the case of swirl ratio of 3.6, which has the Rankine vortex swirl profile, both the turbulence intensity and the turbulence length scale take each maximum value at some measuring points around the cylinder center in the compression stroke. This result was also explained by the calculated result that a middle-scale ring-vortex developed in a region around the cylinder axis generates and transfers turbulence.

ACKNOWLEDGEMENT

Authors would like to express their sincere appreciation to Professors M. Maeda and K. Hishida at Keioh Univ. for their valuable suggestion on LDV instrumentation, and to Professor H. Katakura at Tokyo Technical Univ. for his help supplying experimental instruments. They also thank to Dr. H. Kobayshi and Mr. S. Yamaguchi at Tokyo Institute of Technology for their great help given to this study.

REFERENCES

1. Lancaster, D. R., "Effects of engine variables on turbulence in a spark-ignition engine", SAE paper 760159.
2. Kamimoto, T., Yagita, M., Moriyoshi, Y., Kobayashi, H., and Morita, H., "An experimental study of in-cylinder air flow with a transparent cylinder engine", JSME Int. J., 31-1 Ser. 2 pp. 150-157, 1988.
3. Ikegami M., Shioji M., and Nishimoto K., "Turbulence intensity and spatial integral scale during compression and expansion strokes in a four-cycle reciprocating engine", SAE paper 870372.
4. Kido, H., Wakuri Y., and Murase, E., "Measurements of spatial scales and a model for small-scale structure of turbulence in an internal combustion engine", Proc. of 1983 ASME-JSME Engnrg. Conf., 4 pp. 191-198, 1983.
5. Glover, A.R., Hundleby, G.E., and Hadded, O., "The development of scanning LDA for the measurement of turbulence in engines", SAE paper 880379.
6. Fraser, R.A., and Bracco, F.V., "Cycle-resolved LDV integral length scale measurements in an I.C. engine", SAE paper 880381.
7. Fraser, R.A., and Bracco, F.V., "Cycle-resolved LDV integral length scale measurements investigating clearance height scaling, isotropy, and homogeneity in an I.C. engine", SAE paper 890615.
8. Moriyoshi, Y., Kamimoto, T., Yagita, M., Kobayashi, H., and Morita, H., "Measurement and numerical simulation of in-cylinder air motion of a transparent engine", Trans. Jpn. Soc. Mech. Eng., (in Japanese) 54-502 B, pp. 1541-1548, 1988.
9. Moriyoshi, Y., Kobayashi, H., and Kamimoto, T., "Experimental evaluation of the k-ε turbulence model in numerical simulation of in-cylinder air motion", JSAE Review 10-2 pp. 10-16, 1989.